Free Radical Biology and Medicine 211 (2024) 114–126

Contents lists available at ScienceDirect

Free Radical Biology and Medicine

journal homepage: www.elsevier.com/locate/freeradbiomed

"ATAD3C regulates ATAD3A assembly and function in the mitochondrial membrane"

Paula Gaudó [a], Elena de Tomás-Mateo [a], Nuria Garrido-Pérez [a,b,c,d], Alfredo Santana [e,f], Eduardo Ruiz-Pesini [b,c,**], Julio Montoya [a,b,c], Pilar Bayona-Bafaluy [a,b,c,d,*]

[a] Biochemistry and Molecular Biology Department. Universidad de Zaragoza, 50009- and 50013, Zaragoza, Spain
[b] Institute for Health Research (IIS) de Aragón, 50009, Zaragoza, Spain
[c] Rare Diseases Networking Biomedical Research Centre (CIBERER), 28029, Madrid, Spain
[d] Institute for Biocomputation and Physics of Complex Systems, University of Zaragoza, 50018, Zaragoza, Spain
[e] Research Institute of Biomedical and Health Sciences (IUIBS), University of Las Palmas de Gran Canaria, 35001, Las Palmas de Gran Canaria, Spain
[f] Clinical Genetics Unit, Complejo Hospitarlario Universitario Insular-Materno Infantil de Las Palamas de Gran Canaria, 35016, Las Palmas de Gran Canaria, Spain

ARTICLE INFO

Keywords:
ATAD3C
ATAD3A
ATAD3B
Mitochondria
OXPHOS
Respiratory complexes
Respiratory supercomplexes

ABSTRACT

Mitochondrial ATAD3A is an ATPase Associated with diverse cellular Activities (AAA) domain containing enzyme, involved in the structural organization of the inner mitochondrial membrane and of increasing importance in childhood disease. In humans, two ATAD3A paralogs arose by gene duplication during evolution: ATAD3B and ATAD3C. Here we investigate the cellular activities of the ATAD3C paralog that has been considered a pseudogene. We detected unique ATAD3C peptides in HEK 293T cells, with expression similar to that in human tissues, and showed that it is an integral membrane protein that exposes its carboxy-terminus to the intermembrane space. Overexpression of ATAD3C, but not of ATAD3A, in fibroblasts caused a decrease in cell proliferation and oxygen consumption rate, and an increase of cellular ROS. This was due to the incorporation of ATAD3C monomers in ATAD3A complex in the mitochondrial membrane reducing its size. Consistent with a negative regulation of ATAD3A function in mitochondrial membrane organization, ATAD3C expression led to increased accumulation of respiratory chain dimeric CIII in the inner membrane, to the detriment to that assembled in respiratory supercomplexes. Our results demonstrate a negative dominant role of the ATAD3C paralog with implications for mitochondrial OXPHOS function and suggest that its expression regulates ATAD3A in the cell.

1. Introduction

ATAD3 (ATPase family AAA domain-containing protein 3) is a mitochondrial membrane protein essential for the integrity of mitochondrial inner membrane [1,2]. ATAD3 is a member of the family of ATPases proteins Associated with various cellular Activities (AAA + ATPases) present in metazoans [3,4] and necessary for early embryonic development in *Caenorhabditis elegans* [5], *Drosophila* spp. [6], and mouse [7]. The human ortholog, *ATAD3A*, has been considered one of the five most common genes associated with severe mitochondrial diseases in childhood [8].

The family of AAA + ATPases share a highly conserved AAA domain that determines their assemble into oligomeric complexes, usually hexameric, in the form of a ring with a central channel formed by residues of all the subunits [9–11]. Recent structures of substrate-bound enzymes indicate that the ATPase domains assemble in an asymmetric spiral staircase around the substrate, and that a tightly coordinated sequential cycle of ATP hydrolysis induces conformational changes in the substrate target proteins translocating them through the central pore [12–16]. However, the substrate proteins for ATAD3 ATPases remain elusive.

In cultured mammalian cells ATAD3 has been implicated in a variety of functions: mtDNA organization and segregation [4,17–21]; mitochondrial morphology and dynamics, including fusion, fission,

* Corresponding author.Departamento de Bioquímica, Biología Molecular y Celular. Facultad de Ciencias, Universidad de Zaragoza, C/ Pedro Cerbuna, 12. 50009, Zaragoza, Spain
** Corresponding author.Rare Diseases Networking Biomedical Research Centre (CIBERER). C. de Melchor Fernández Almagro, 3. 28029, Madrid, Spain
E-mail addresses: eduruiz@unizar.es (E. Ruiz-Pesini), pbayona@unizar.es (P. Bayona-Bafaluy).

https://doi.org/10.1016/j.freeradbiomed.2023.12.006
Received 7 June 2023; Received in revised form 28 November 2023; Accepted 7 December 2023
Available online 12 December 2023

biogenesis, and mitophagy [6,20,22,23]; cholesterol transfer between endoplasmic reticulum (ER) and mitochondria [6,24]; and steroidogenesis [25,26]. The study of muscle- and neuron-specific knockout mouse models established that disruption of mitochondrial cristae structure is the first phenotype associated with ATAD3 loss. Other processes coupled to membrane organization, such as mtDNA replication, respiratory supercomplexes (SC) abundance and cholesterol metabolism, were secondarily affected, probably as a consequence of the role of ATAD3 in the organization of protein complexes in the inner mitochondrial membrane [1,2].

In humans, three *ATAD3*-derived genes *ATAD3A*, *ATAD3B*, and *ATAD3C* are annotated at the same locus on human chromosome 1. During evolution, the ancestral gene, *ATAD3A*, was duplicated in tandem giving rise to a close paralogue with an extension at the carboxy terminus, *ATAD3B*, and a truncated paralogue, *ATAD3C* [3,27]. The locus has been implicated in a rapidly increasing number of cases of pediatric-onset mitochondrial diseases, highlighting the relevance of ATAD3 in mitochondrial physiology. *ATAD3A* is the major disease-associated gene [22,23,28,29]. However, the high homology between the three genes in the region facilitates genomic rearrangements. Thus, recessive deletions and dominant duplications causing fatal perinatal mitochondrial disease have been recently described in the region [25,30–32]. It is unclear, however, the cellular importance of ATAD3A paralogs. Although a specific role in mitophagy has been proposed for ATAD3B [33], it could form hetero-oligomers with ATAD3A [34]. No experimental information is available on ATAD3C.

Gene duplication followed by functional specialization is one of the primary forces by which novel gene functions can arise [35,36]. Within the proteome, duplications are enriched for protein families with certain domains, including the AAA + ATPase domain [35]. The role of the majority of the hominid-specific duplicated genes remains unknown, and many could be non-functional or redundant with their ancestral form [37]. However, examples of gene duplications including truncated genes that contributed to human brain development have recently been described [38–40].

Given the increasing importance of the human *ATAD3* locus in mitochondrial disease, we further analyzed the specific ATAD3C paralog. We found that ATAD3C can interact with ATAD3A and incorporate into the main ATAD3A assembly in the mitochondrial membrane reducing its size. Through molecular and functional analysis, we found evidence that ATAD3C but not ATAD3A expression in fibroblasts leads to accumulation of dimeric complex III by reducing its incorporation into respiratory supra-molecular structures or SC reducing cellular proliferation and cellular respiration. These data suggest that the paralog ATAD3C has the potential to negatively regulate ATAD3A function in the mitochondrial inner membrane organization and its expression levels in certain tissues should be considered in association with human diseases.

2. Material and methods

2.1. Cell culture and cell transduction

Primary human fibroblasts derived from the skin of 1-month-old (Fb (1)), 3-year-old (Fb(3)) and 3.5-year-old (Fb(3.5)) subjects were obtained from Hospital San Joan de Déu Barcelona. Human Kidney embryonic cell line HEK 293T, neuroblastoma cell line SH-SY5Y, and fibroblasts were propagated in either high-glucose DMEM (25 mM glucose), low-glucose DMEM (5 mM glucose), or in DMEM no glucose (Gibco-Thermo Fisher Scientific) supplemented with 5 mM galactose and 1 mM sodium pyruvate (DMEM galactose). RPMI 8226 cells were propagated in RPMI medium (Gibco-Thermo Fisher Scientific). All media were supplemented with 10 % (v/v) fetal bovine serum (Thermo Fisher Scientific) and cells maintained at 37 °C in a 5 % (v/v) CO_2 atmosphere.

Cell transduction was carried out using a lentiviral system as previously described [41]. Lentiviral particles were generated in HEK 293T packaging cells by co-transfection of the gene expression constructs, with the packaging psPAX2 (Addgene plasmid #12260) and envelope pMD2.G (Addgene #12259) plasmid. To generate stable ATAD3 expressing cells, sub-confluent cells were transduced using lentiviral particles, and stably expressing cells were selected using puromycin (final concentration of 2.5 μ g/ml for HEK 293T cells and 0.25 to 0.4 μ g/ml for fibroblasts) over a period of 10 days. When indicated, primary skin fibroblasts were immortalized by lentiviral transduction of pLOXTtag-iresTK plasmid (Addgene #12246).

2.2. Gene expression constructs

ATAD3A transcript variant 2 (NM_001170535.3; Q9NVI7-2) was amplified and cloned from HEK 293T total RNA; *ATAD3C* (NM_001039211.3; Q5T2N8), was amplified and cloned from RPMI 8226 total RNA; and *ATAD3B* transcript variant 1 (NM_031921.6; Q5T9A4-1) was obtained from Dharmacon™ cDNA Clones, GE Healthcare. See Table S1 for transcript variants. Open reading frames (ORF) were PCR-amplified from cDNA using Phusion Hot Start II DNA Polymerase (Thermo Fisher Scientific) and primers: *ATAD3A* Fw: GTTTAAACGCCACCATGTCGTGGCTCTTCG and *ATAD3A* Rv: GGATCCTCAGGATGGGGAGGGCTCG for *ATAD3A*, *ATAD3B* Fw: GTTTAAACATGTCGTGGCTCTTCGGCATTAAC and *ATAD3B* Rv: GGATCCCTACAACAGGGGGTGCCCT for *ATAD3B*, and *ATAD3C* Fw: GTTTAAACGCCACCATGTCAAAGGACGCCCTGA and *ATAD3C* Rv: GGATCCTCAGGATGAGGGTTGCTCG) for *ATAD3C*. Amplified products were cloned using the Zero Blunt™ TOPO™ PCR Cloning Kit (Invitrogen). To add HA-tags, the ORF were re-amplified including the HA coding sequence in the reverse primer (carboxyl terminus of the protein) except for ATAD3C-HA(N) in which HA epitope was added with the forward primer. Expression constructs in lentiviral pWPXLd-ires-PuroR target vector (version of pWPXLd, Addgene #12258) were obtained by restriction enzyme digestion with *Pme*I and *Bam*HI and T4 DNA ligase mediated ligation.

2.3. Assessment of cell proliferation rate

Incucyte® SX5 Live-Cell Analysis System (Essen Bioscience) was used for monitoring cell proliferation. Cells were seeded in 96-well plates at 1×10^4 cells per well in high-glucose DMEM or DMEM galactose. Phase contrast images of the well were obtained every 12 h for a total period of 4 days. Measurements of cell growth were based on occupied area (confluence).

2.4. High-resolution respirometry

Exponentially growing cells were collected by trypsinization, and resuspended at 1×10^6 cells/ml in high-glucose DMEM. Oxygen consumption was monitored for 15 min at 37 °C using OROBOROS Oxygraph (Anton Paar, Innsbruck, Austria), with chamber volume set at 2 ml. The software DatLab was used for data acquisition at 1 s time intervals, as well as for data analysis.

2.5. Flow cytometry estimation of ROS production

$1{,}5 \times 10^5$ cells were seed in 6 wells plates in low glucose medium. 24 h latter 2′,7′-dic hlorodihydrofluorescein diacetate (DCFH-DA) (5 μ M) or MitoSOX™ Red (1 μ M) probes (Invitrogen™) were added in HBSS medium for 30 min at 37 °C. Cells were collected by tripsinization and

simple fluorescence measurements were performed in a GALLIOS cytometer (Beckman Coulter). Control samples were treated with100 μ M oxygen peroxide for 10 min after tripsinization or with1 μ M rotenone for 30 min in culture.

2.6. Reverse transcription and quantitative qPCR

Total RNA was isolated using TRIzol® reagent (Invitrogen). First-strand cDNA was synthesized from 1 μg of total RNA with Transcriptor First Stand cDNA Synthesis Kit (Roche). Relative quantification was performed using TaqMan Gene Expression Assays in a Viia 7 system (Applied Biosystems™) according to the manufacturer's instructions. Actin was used as reference gene. TaqMan probes used were: *ATAD3A* (Hs01587333_m1, # 4331182); *ATAD3B* (Hs02577779_Mh, #4331182); *ATAD3C* (Hs03008589_g1, #4351372); *β-Actin* (Hs99999903_m1, #4333762T). Superoxide dismutase [Mn] (*SOD2*) and catalase (*CAT*) expression were quantified using PowerUp™ SYBR™ Green Master Mix (Thermo Fisher Scientific) and the primer pairs: hSOD2-F, TCAGGATCCACTGCAAGGAA, hSOD2-R CGTGCTCCCACACATCAATC and hCAT-F GGCCTTTGGCTACTTTGAGG, hCAT-R CCGATTCTCCAGCAACAGTG respectively. Actin was used as a reference, hACTB-F ccaaccgcgagaagatga and hACTB-R ccagaggcgtacagggatag.

2.7. Mitochondrial isolation and sub-fractionation

Mitochondrial fractions were isolated from HEK 293T cells essentially as described previously [42] and from human fibroblasts as described [43]. To prepare submitochondrial fractions, freshly isolated mitochondria were resuspended in (10 mM Tris-Cl, 100 mM NaCl, pH 7.4) at a protein concentration of 5 mg/ml. After 5 cycles of freeze-thawing were either sonicated (UP 200S Ultrasonic Processor, Hielscher) or treated with 100 mM Na_2CO_3 (pH 11.3), and centrifuged for 1 h, 18 000×*g* at 4 °C. The resulting supernatant and pellet fractions were subsequently dissolved and/or mixed with SDS–PAGE sample buffer. For the protease protection assay, freshly isolated mitochondria (~11 μ g of protein) were resuspended in TL buffer (30 mM Tris-HCl, pH 7.4, 4 mM Mg-acetate, 5 mM ε-amino-n-caproic acid, 50 mM NaCl, 1 mM ATP) and incubated for 20 min at 25 °C with trypsin (final concentration 50 μ g/ml) and with increased amounts of digitonin (0, 25, 75, 150, 300 and 900 μ g) to progressively dissolve the outer and the inner mitochondrial membranes. Subsequently, the samples were incubated with DNase at room temperature for an additional 5 min. A control sample to assess the integrity of the mitochondria was treated with trypsin but not digitonin. The control for complete protein digestion was treated with trypsin in the presence of 1 % Triton X-100. Trypsin digestion was stopped by 25 μ l of PBS with 10 % FBS, and the samples were routinely processed for SDS–PAGE.

2.8. Coimmunoprecipitation experiments

For anti-HA coimmunoprecipitation, mitochondria (~200 μ g of protein) were solubilized with 1 % digitonin in Solubilization Buffer (50 mM Tris HCl pH 7.4, 150 mM NaCl, 10 % glycerol, 1 mM EDTA,1 % protease inhibitor cocktail (EASYpack, Roche)) at a protein concentration of 5 mg/ml, 30 min at 4 °C with gentle agitation. Non-solubilized material was removed by centrifugation at 10 000×*g*, for 10 min at 4 °C, and 1 volume of solubilization buffer without digitonin was added to the supernatant. The extracts were incubated for 2 h and 30 min at 4 °C with gentle agitation with 0.2 mg of anti-HA-magnetic beads (Pierce Anti-HA Magnetic Beads). Magnetic beads were previously washed 3 times with Washing Buffer (50 mM Tris HCl pH 7.4, 150 mM NaCl, 10 % glycerol, 1 mM EDTA, 0.2 % digitonin, and 1 % protease inhibitor cocktail). The magnetic beads containing bound immunocomplexes were washed ten times with Washing Buffer and next incubated with sample buffer (20 % glycerol (v/v), 8 % SDS, 0.04 % Bromophenol blue (p/v), 0.16 M Tris HCl pH 6.8) at 95 °C for 5 min to denature and release the immunocomplexes.

2.9. Liquid chromatography mass spectrometry (see supplementary methods)

2.9.1. SDS-PAGE, BN-PAGE and Western blot

Electrophoresis and Western blotting were performed using standard methods. For SDS-PAGE, total cell protein was extracted with RIPA buffer (MILLIPORE) and 30–40 μ g of protein was loaded in polyacrylamide gels between 7 % and 14 %. 1D-BN-PAGE was performed as described previously [44]. Briefly, mitochondrial proteins (~200 μg of protein) were solubilized with 1.5 % (w/v) digitonin in TL buffer (30 mM Tris-HCl, pH 7.4, 4 mM Mg-acetate, 5 mM ε-amino-n-caproic acid, 50 mM NaCl, 1 mM ATP) with 1 % protease inhibitor cocktail (EASYpack, Roche) at a protein concentration of 5 mg/ml (in 40 μl) by incubation in an orbital shaker for 20 min at 4 °C, then centrifuged for 20 min, 13 000×*g*, at 4 °C, and the supernatant was mixed with BN–PAGE sample buffer. Pre-cast NativePAGE™ 3–12 % gradient Bis-Tris Protein Gels (Invitrogen™), NativePAGE™ Running Buffer and NativePAGE™ Cathode Buffer Additive (Novex®, Life technologies), sample buffer 5X (5 % of Blue G-250 in 0.75 M aminocaproic acid, 50 mM Bis-Tris/HCl pH 7) and NativeMark™ Unstained Protein Standard (Invitrogen™) were used. For 2D-SDS-PAGE, the lanes of the 1D Blue Native gel were cut out, incubated for 1 h at room temperature in water with 1 % SDS and 1 % β-mercaptoethanol, and arranged horizontally in the single well of an SDS-PAGE-Tricine gel. Blots were obtained using wet electro-transference (Trans-Blot Cell, Bio-Rad) and were developed using Western Blotting Substrate (Pierce). Western blot signals were acquired using Amersham imager 600 system (GE Healthcare Life Science). The resulting digital images were analyzed using the ImageQuantTL Amersham (GE Healthcare Life Science).

2.9.2. Antibodies

Polyclonal antibodies were used against: ATAD3A (Sigma, #SAB1400606-50UG); ATAD3A (Abnova, #H00055210-D01, only when indicated); ATAD3B (Sigma, #HPA058968); complex III iron-sulfur subunit, UQCRFS1 (Invitrogen, #PA521420). Monoclonal antibodies were used against: HA (Roche, #11867423001); complex II subunit SDHA (Thermo Fisher Scientific, #459200); complex II subunit SDHB (Thermo Fisher Scientific, #459230); complex III subunit UQCRC2 (Abcam, #ab14745); ATP synthase subunit C, ATP5MC1 (Abcam, #ab181243); ATP synthase subunit alpha, ATP5A1 (Invitrogen, #459240); complex IV subunit I, COX1 (Thermo Fisher Scientific, #459600); complex I subunits: NDUFA9 (Thermo Fisher Scientific, #459100) and NDUFB8 (Thermo Fisher Scientific, #459210); TOM20 (SantaCruz biotechnology, #Sc11415); VDAC1 (Abcam, #14734); Hsp60 (Sigma, #H4149); α-Tubulin (Sigma, #T6074). Total OXPHOS Human WB Antibody Cocktail (Abcam, #ab110411).

2.10. Statistical analysis

Statistical analyses were performed using non-parametric Mann-Whitney *U* test (StatView 5.0). The results are expressed as mean ± SD; $p < 0.05$ was considered statistically significant. Experiments were performed at least in triplicate.

3. Results

3.1. ATAD3C retains the AAA domain structure of ATAD3A and ATAD3B

To estimate when the evolutionary duplication occurred at the *ATAD3* locus, we searched the NCBI Reference sequence (RefSeq) database [45] for the terms "ATAD3C" and "ATPase family AAA domain-containing protein 3C". In animals, the gene is present in two

families of primates, the Cercopithecidae and the Hominidae, indicating that the duplication event occurred before Great Apes and Old-World Monkeys divided 25 million years ago [46].

ATAD3C contains an open reading frame and encodes a protein homologous to ATAD3A and ATAD3B but truncated in the N-terminal region. The truncated protein retains the characteristic AAA + domain (Fig. 1A, Supplementary Fig. S1). Based on structural topology the AAA + domain consists of a wedge-shaped subdomain that has β-sheets of parallel strands, arranged in a β 5– β 1– β 4– β 3– β 2 sequence at its core, connected by loops of short α-helices and a conserved α-helical bundle at the C terminus [10,47]. The tridimensional ATAD3C folding, obtained with the AlphaFold algorithm [48], matched with the predicted folding for ATAD3A and ATAD3B and preserved the structural integrity of its AAA + domains (Supplementary Fig. S2).

Using the BLAST program [49], we search for human AAA + family members with high homology with ATAD3C. The closest relatives of *ATAD3C* were its paralogs *ATAD3A* and *ATAD3B,* followed by proteins of the subfamily of AAA ATPases, mainly from three of the six major clades: the MSP1/katanin/spastin group, the proteasome subunits, and the metalloproteases clade (Supplementary Tables S2, S3 and S4). In addition to the distinctive Walker A and B motifs in the ATP binding region of the AAA domain, the AAA subfamily contains a conserved arginine downstream of the Walker B motif and a highly conserved motif, the Second Region of Homology (SRH) adjacent to the arginine finger (arginine position 1) [9,11,50]. Clustal alignment of t human ATAD3 paralogs and several members of the AAA subfamily showed that ATAD3A, ATAD3B and ATAD3C protein sequences contain the common motifs, except for the arginine at position 2. Instead they contain the arginine at position 3 (Fig. 1B). Remarkably, ATAD3C lacks the arginine finger that is highly conserved in most AAA + proteins with only minor exceptions [11,50]. The predicted hydrogen bonds of arginines 1 and 4 with other protein residues differ among paralogs (Supplementary Fig. S3).

Collectively, these results indicate that ATAD3 protein paralogs belong to the AAA subfamily of AAA + ATPases and suggest that ATAD3C, despite being truncated relative to ATAD3A, could generate a correctly folded AAA protein.

3.2. *ATAD3C expression is lower than that of ATAD3A and ATAD3B in human tissues and cell lines*

Data from RNA-seq analyses on 50 human tissues from the *Genotype-Tissue Expression (GTEx)* project [51], collected at the expression Atlas [52], revealed similar but distinct expression patterns for *ATAD3A* and its paralogs trough the tissues (Fig. 1C). *ATAD3A* and *ATAD3B* were expressed in all tissues tested, with absolute levels of expression in transcripts per million (TPM) ranging from 7 to 30 TPM for *ATAD3A* and from 4 to 28 TPM for *ATAD3B* (being medium level between 11 and 1000 TPM; low level between 0.5 and 10 TPM; and cutoff below 0.5 TPM). *ATAD3C* expression levels were overall lower, from 0.4 to 11 TPM, with thyroid and prostate glands, tibial nerve and C1 segment of cervical spinal cord showing the highest expression. Six tissues, including transformed skin fibroblasts, displayed levels of expression of *ATAD3C* close to or below the detection threshold (Fig. 1C). Interestingly, the Human Developmental Biology Resource (HDBR) [52,53] detected *ATAD3C* expression during prenatal human brain development with the highest expression in forebrain at 13 post conception weeks (12 TPM vs. *ATAD3A* 18 TPM). In general, the relative amount of expression of each paralog throughout human tissues was A $\geq$ B > C (Fig. 1C). A similar trend was observed in cell lines, analyzing RNA-seq datasets obtained from the *Human Protein Atlas* [54], with the exception of the RPMI 8226 cell line (B lymphocytes obtained from a plasmacytoma patient) that shows higher expression *of ATAD3C* than *of ATAD3B* (Fig. 1D).

We used highly specific quantitative TaqMan real-time PCR assays to measure the expression of the *ATAD3* paralogs in three selected immortalized human cell lines, HEK 293T, RPMI 8226 and SH-SY5Y, and in primary human-derived fibroblasts (Fb). The relative expression of *ATAD3A* and *ATAD3B* among cell lines was comparable with that detected in RNAseq experiments (Fig. 1 E). However, we only detected *ATAD3C* expression in RPMI-8226 cells (Fig. 1F). Under conditions of mitochondrial biogenesis (galactose medium), qPCR assays detected an increase in the relative steady-state levels of *ATAD3A* and *ATAD3B* transcripts in immortalized cells but not in primary cells (Fig. 1 G). Under these conditions, ATAD3C was also detected only in the RPMI 8226 cell line. Consistent with its higher expression, we were able to clone the *ATAD3C* transcript (NM_001039211.3) encoding a 46.4 kDa protein (Q5T2N8) from this cell line but not from HEK 293T or SH-SY5Y.

In conclusion, at the human *ATAD3* locus, *ATAD3C* is not ubiquitously expressed in human tissues and its expression is usually lower than the expression of its paralogs. However, some tissues show medium expression levels in TPMs.

3.3. *ATAD3C is translated into a mitochondrial outer membrane protein in cultured cells*

We next used mass spectrometry (MS) to determine whether the *ATAD3C* gene produces a protein. Using a targeting approach, two unique ATAD3C peptides were detected in HEK 293T cells, consistent with gene expression detected by RNAseq in the cell line. MS failed to identify unique ATAD3C peptides in fibroblasts, in which gene expression was not detected by RNAseq (Supplementary Fig. S4). In these experiments, several unique peptides of ATAD3A (isoform 2, Q9NVI7-2) and ATAD3B (isoform 1, Q5T9A4-1) respectively were detected in both cell types (Supplementary Table S1, Supplementary Figs. S4 and S5).

Using a lentiviral system, we stably expressed a hemagglutinin-tagged version of ATAD3C (ATAD3C-HA) in the HEK 293T cell line (HEK 293T-ATAD3C-HA). In a subsequent immunoblot of whole-cell lysate, a band was detected with anti-HA immunoreactivity at the expected size (theoretical mass: 47.5 kDa) confirming that the *ATAD3C* ORF generates a protein (Fig. 2A). To examine the relative steady-state levels of ATAD3 proteins in HEK 293T cells, we used commercial antibodies raised against ATAD3A and ATAD3B. Given the high sequence similarity between ATAD3 paralogs, the antibodies did not exclusively detect the protein they were raised against. Two close bands appeared when using specific anti-ATAD3A antibodies, the more intense one corresponding to ATAD3A at the expected size (isoform 2, theoretical mass: 66.2 kDa) and the less intense consistent with the ATAD3B protein (isoform 1, theoretical mass of 72.6 kDa). Two bands appeared also with an antibody raised against ATAD3B being more intense the upper one considered ATAD3B. Cells expressing the main transcript for each paralog, or its HA-tagged version, were used as controls in immunoblot detections (Fig. 2A). Remarkably, the antibodies tested against ATAD3A or ATAD3B did not detect any band of the size expected for ATAD3C.

ATAD3C possess a putative mitochondrial leader sequence (TM1) that is common for the three ATAD3 paralogs and could direct its import into mitochondria (Fig. 1A) [6]. By cell sub-fractionation we confirmed that ATAD3C-HA was found highly enriched in mitochondrial fractions of HEK 293T cells. To determine in which mitochondrial fraction, soluble or membranous, mitochondria isolated from HEK 293T cells overexpressing ATAD3C-HA were subjected to either sonic treatment or alkaline carbonate extraction. Sonic treatment showed that ATAD3C is a membrane protein (Fig. 2B). Upon alkaline extraction of mitochondrial membranes at pH 11.3, ATAD3C-HA behaved like VDAC1 or UQCRFS1 (markers of outer (OMM) or inner (IMM) mitochondrial membrane, respectively) indicating tight association with the membrane. HSP60 and SDHA proteins, that lack transmembrane domains, were used as markers of soluble protein (HSP60), or weakly associated with the membrane (SDHA), and, as expected, were extracted from the membrane at high pH (Fig. 2B). To further define the submitochondrial location, we took advantage of the HA epitope located either at the amino- or the carboxy-terminus of ATAD3C. Mitochondria isolated from

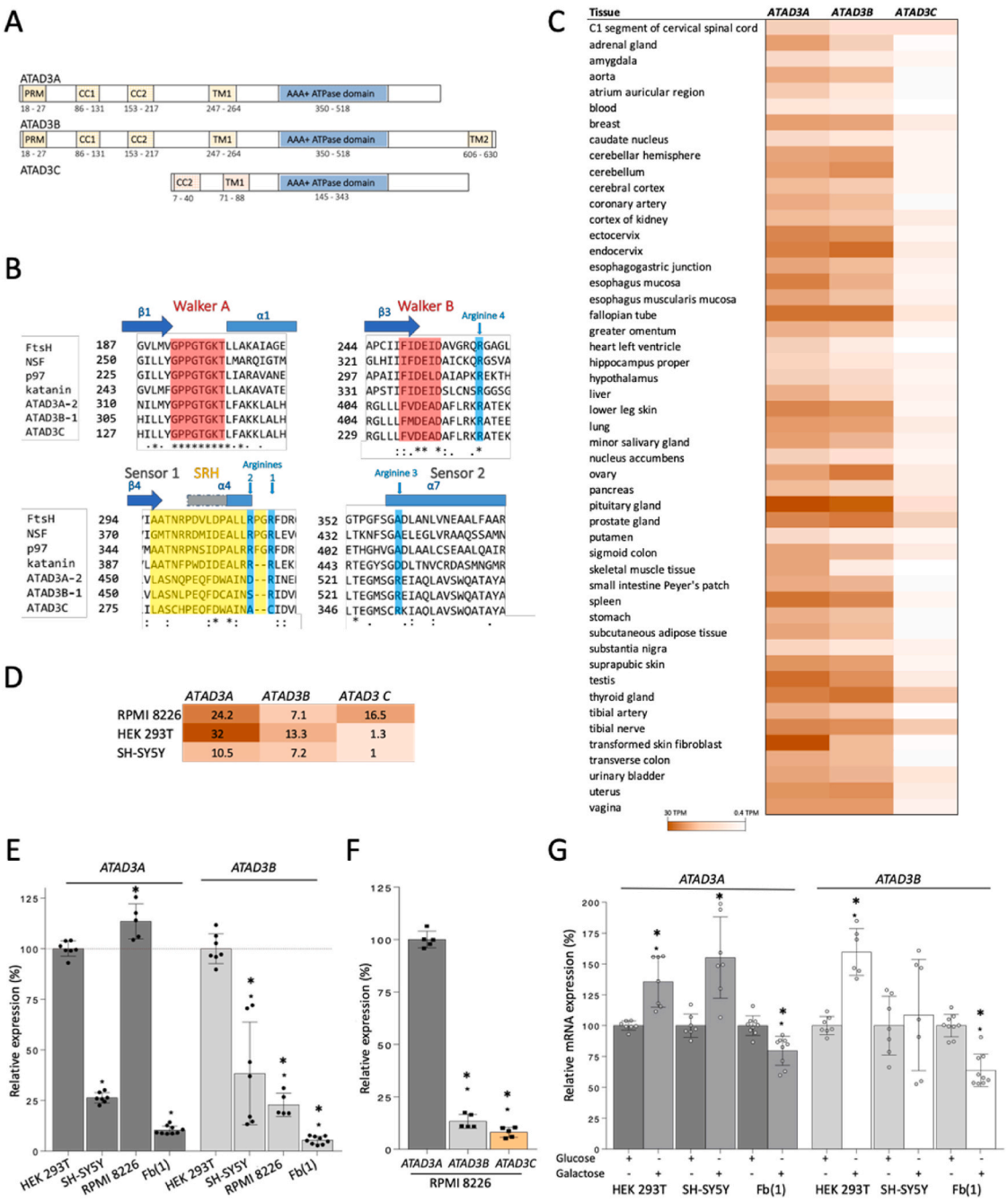

Fig. 1. ATAD3C share conserved domains with ATAD3A and ATAD3B although its expression is lower in tissues and in most cell lines.

A. Schematic representation of human ATAD3C, ATAD3A and ATAD3B predicted protein domains. A flexible proline-rich region (PRM), two predicted coiled-coil domains (CC1 and CC2), the predicted transmembrane sequences (TM1 and TM2), and the AAA + ATPase domain conserved in the AAA + protein family, are indicated. The NPS@ Web server was used for the predictions [55].

B. Fragment alignment of several proteins of the AAA ATPase subfamily in Blastp highlighting the main conserved residues. Walker A and B motifs and the second region of homology (SRH) are highlighted in red and yellow, respectively. Arginine finger (position 1) and other conserved arginines (positions 2, 3 and 4) are colored in blue. Beta sheet and alpha helices are indicated.

C. *ATAD3A*, *ATAD3B* and *ATAD3C* expression data in 50 human tissues obtained by RNA-seq analyses from the *Genotype-Tissue Expression (GTEx)* project.

D.*ATAD3A*, *ATAD3B* and *ATAD3C* expression data in cell lines, obtained by RNA-seq analyses in the *Human Protein Atlas.*

E. Relative expression of *ATAD3A*, *ATAD3B* and *ATAD3C* mRNAs in cell lines. Expression data obtained by qPCR are presented as mean ± SD. *ATAD3C* expression was below the detection threshold. The asterisks represent the significance level calculated by non-parametric Mann-Whitney *U* test, *p < 0.05 (vs. *ATAD3A* expression in HEK 293T cell line, considered 100 %, dashed line).

F. Expression of *ATAD3A*, *ATAD3B* and *ATAD3C* mRNAs in RPMI 8226 cells. Expression data obtained by qPCR are presented as mean ± SD. The asterisks represent the significance level calculated by non-parametric Mann-Whitney *U* test, *p < 0.05 (vs. *ATAD3A* expression considered 100 %).

G. Relative expression of ATAD3A, ATAD3B and ATAD3C mRNAs in cell lines under conditions of mitochondrial biogenesis. Glucose and galactose indicate the monosaccharide present in the cell culture medium. Data are presented as mean ± SD. *ATAD3C* expression was below the detection threshold. The asterisks represent the significance level calculated by non-parametric Mann-Whitney *U* test, *p < 0.05 (vs. expression in the same cell line grown in glucose).

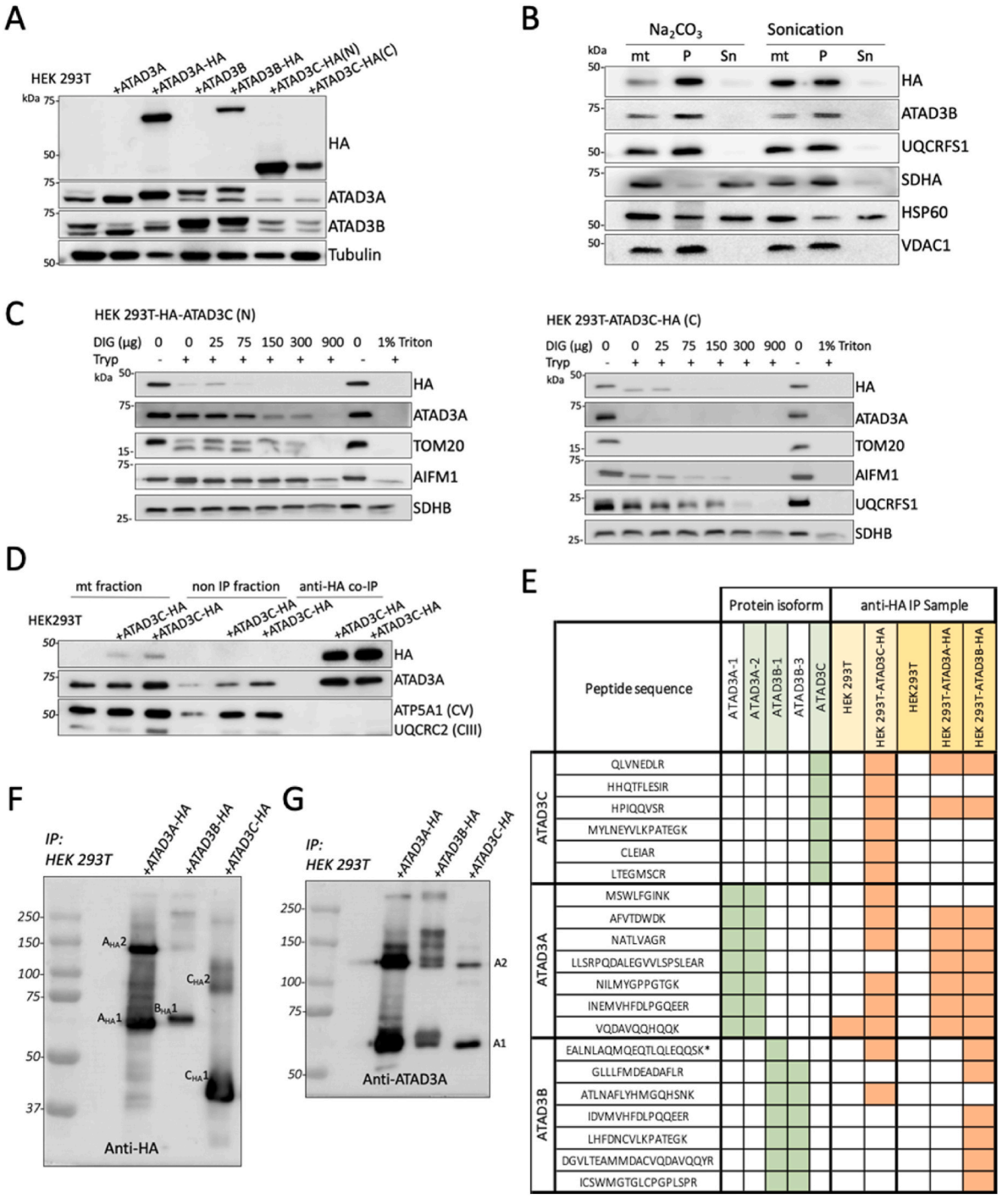

(caption on next page)

Fig. 2. *ATAD3C* is translated into a mitochondrial outer membrane protein that interacts with ATAD3A
A. SDS–PAGE analysis of HEK 293T and HEK 293T overexpressing ATAD3A, ATAD3B and ATAD3C proteins or HA tagged versions. β-Tubulin was used as loading control. HA, hemagglutinin epitope. N and C indicate location of the HA epitope in the amino- or carboxy-terminal end of ATAD3C.
B. Sub-mitochondrial localization of ATAD3C. Mitochondria (mt) were isolated from HEK 293T cells overexpressing ATAD3C-HA and disrupted by sonication or extracted with sodium carbonate and separated into pellet (P) and supernatant (Sn) fractions by centrifugation. Fractions were analyzed by SDS–PAGE and immunoblotting. HSP60 served as a soluble protein marker, VDAC1 and UQCRFS1 as membrane embedded protein markers and SDHA as associated membrane protein marker.
C. Sub-mitochondrial topology of ATAD3C-HA. Mitochondria were isolated from HEK 293T cells overexpressing ATAD3C tagged with the -HA epitope in the amino (N) or carboxy-terminal end (C) and treated in the absence or presence of increasing amounts of digitonin, trypsin (50 μg/ml), or triton-X100 (1 %), as indicated. Fractions were analyzed by SDS–PAGE and immunoblotting. TOM20 served as outer mitochondrial membrane marker (OMM), AIF as intermembrane space marker (IMS); UQCRFS1 as inner mitochondrial membrane marker (IMM) facing the IMS, and SDHB as a protein facing the matrix.
D. SDS-PAGE analysis of proteins immunoprecipitated with anti-HA-conjugated magnetic beads. HEK 293T and HEK 293T-ATAD3C-HA isolated mitochondria were subjected to anti-HA immunoprecipitation, and fractions were separated by SDS–PAGE and immunodetected sequentially with specific antibodies (anti-HA, anti-ATAD3A and OXPHOS antibody cocktail).
E. Unique peptides of ATAD3A, ATAD3B and ATAD3C proteins detected by LC-MS/MS in samples subjected to immunoprecipitation with anti-HA magnetic beads. The isoforms of the ATAD3 paralogs to which the detected peptides correspond are indicated in green and the cell lines in which they have been found are indicated in orange.
F., G. Analysis of ATAD3A, ATAD3B and ATAD3C oligomer formation by non-reducing SDS-PAGE in HEK 293T cells and HEK 293T overexpressing ATAD3 paralogs. Co-IPs of HEK 293Tcells, or HEK 293T expressing ATAD3A-HA, ATAD3B-HA or ATAD3C-HA were separated by SDS–PAGE in non-reducing conditions and immunodetected with anti-HA antibody (F) and anti-ATAD3A antibody (Abnova) (G). $A_{HA}1$ and $A_{HA}2$ indicate ATAD3A-HA monomer and dimer respectively. $B_{HA}1$ indicates ATAD3B-HA monomer. $C_{HA}1$ and $C_{HA}2$ indicate ATAD3C-HA monomer and dimer respectively. A1 and A2 indicate endogenous ATAD3A monomer and dimer respectively.

HEK 293T-ATADC3-HA cells were subjected to the disruption of the outer mitochondrial membrane with increasing doses of digitonin and the sensitivity of HA to externally added trypsin was assessed. When the amino-terminus was HA tagged (N) it behaved similarly to TOMM20 (OMM protein), but not to AIFM1 (intermembrane space protein, IMS), or SDHB (mitochondrial matrix protein), indicating that it could be exposed to the cytosol. Interestingly, in this assay ATAD3A also behaved like an OMM protein (Fig. 2C). When the ATAD3C carboxy-terminus was HA-tagged (C), the HA immunoblot signal was found to be highly sensitive to protease addition compared with a matrix protein (SDHB). It was comparable to that of an IMS protein, AIFM1, (Fig. 2C), indicating that the carboxy -terminus is exposed within the IMS.

We concluded from these results that human ATAD3C is an integral membrane protein that exposes its carboxy-terminus to the intermembrane space and its protruding amino-terminus to the cytosol.

3.4. *ATAD3C dimerizes and interacts with ATAD3A*

AAA ATPase domains are involved in dimerization and further oligomerization is required for protein activity. To gain insight into the oligomerization capacity and possible interactions of ATAD3C with its paralogs, we carried out anti-HA immunoprecipitation (IP) under non-denaturing conditions using HEK 293T-ATAD3C-HA isolated mitochondria. Western blot screen of the samples demonstrated that ATAD3A co-immunoprecipitated (co-IP) with ATAD3C-HA, indicating physical interaction, whereas several mitochondrial respiratory chain proteins (UQCRC2 and ATPA51) were detected in the non-IP fraction (Fig. 2D). The subsequent examination of the co-IP products by immunodetection and MS found ATAD3A and ATAD3B in the ATAD3C-HA co-IP (Fig. 2E and Supplementary Fig. S6).

We next carried out anti-HA IP of mitochondria isolated from HEK 293T cell lines overexpressing either ATAD3A-HA or ATAD3B-HA, and analyzed all the co-IP fractions using non-reducing SDS-polyacrylamide gels. The anti-HA antibody detected ATAD3A-HA in two bands one corresponding to the monomer at the expected size of around 67 kDa (theoretical mass: 67.3 kDa), and the other one migrating a little slower consistent with a dimer (theoretical mass: 134.6 kDa) (Fig. 2F). The pattern matches that observed for endogenous ATAD3A (Fig. 2G). In the blot, ATAD3B-HA was found mainly as a monomer (theoretical mass: 73.7 kDa), and ATAD3C-HA was found in a band corresponding to a monomer (theoretical mass: 47.5 kDa) and a second band, showing a smear that could contain a dimer (theoretical mass: 95 kDa) but could also indicate dimerization of ATAD3C with its higher molecular weight paralogs (Fig. 2F). Endogenous ATAD3A was found in the co-IPs of the three paralogs (Fig. 2G). Subsequent examination of the co-IP products by MS found that just as ATAD3A and ATAD3B co-IP with ATAD3C-HA, the reverse was also true, endogenous ATAD3C interacted with ATAD3A-HA and ATAD3B-HA. Under these conditions, we did not find interaction of ATAD3B with ATAD3A-HA (Fig. 2E and Supplementary Fig. S6).

In conclusion, ATAD3C-HA could physically interact with both ATAD3A and ATAD3B but showed less tendency to form homodimers than ATAD3A suggesting a possible regulatory role for ATAD3C by forming heterodimers with its paralogs.

3.5. *Human fibroblasts expressing ATAD3C exhibited reduced growth rate, diminished cell respiration and increased ROS production*

In an attempt to characterize the physiological significance of the interaction of ATAD3C with its paralogs, we used a gain-of-function approach in primary human derived skin fibroblasts. The HA-tagged versions of the three ATAD3 paralogs were expressed in fibroblasts. Western blot screen of whole-cell lysates showed a robust expression for ATAD3A-HA and ATAD3C-HA (Fig. 3A). The steady-state levels of multiple OXPHOS subunits: ATP5MC1 of CV, UQCRC2 of CIII, NDUFB8 of CI, and COX1 of CIV, were similar to those of control cells in all the cases (Fig. 3A). MitoTracker staining and fluorescence microscopy showed that HA staining matched the mitochondrial reticulum in the cells expressing ATAD3A-HA or ATAD3C-HA (Supplementary Fig. S7). ATAD3B-HA expression was not detected by immunocytochemistry. Transmission electron microscopy images generally revealed normal mitochondrial cristae in the gain-of-function cells (Supplementary Fig. S8).

To assess the overall effect on cell viability, we measured the growth rates of control and ATAD3 overexpressing fibroblasts over a time course of 5 days. We found significant growth retardation associated with the overexpression of ATAD3C-HA when galactose medium was used, suggesting that the protein expression interferes with normal cell proliferation when oxidative phosphorylation is required (Fig. 3B). In agreement, oxygen consumption was significantly reduced in fibroblasts overexpressing ATAD3C-HA, whereas overexpression of ATAD3A-HA did not modify cell respiration (Fig. 3C). No decrease in mtDNA levels was detected in the overexpressing cells (Supplementary Fig. S9).

Since the respiratory chain is an important site of superoxide radical anion ($O_2^{\bullet}-$) [56], we performed an assessment of the cellular redox state using DCFH-DA probe. Fb(1) overexpressing ATAD3C-HA showed significantly higher DCFH oxidation, indicating that reactive oxygen species (ROS) are increased in this cell line (Fig. 3D). MitoSOX oxidation

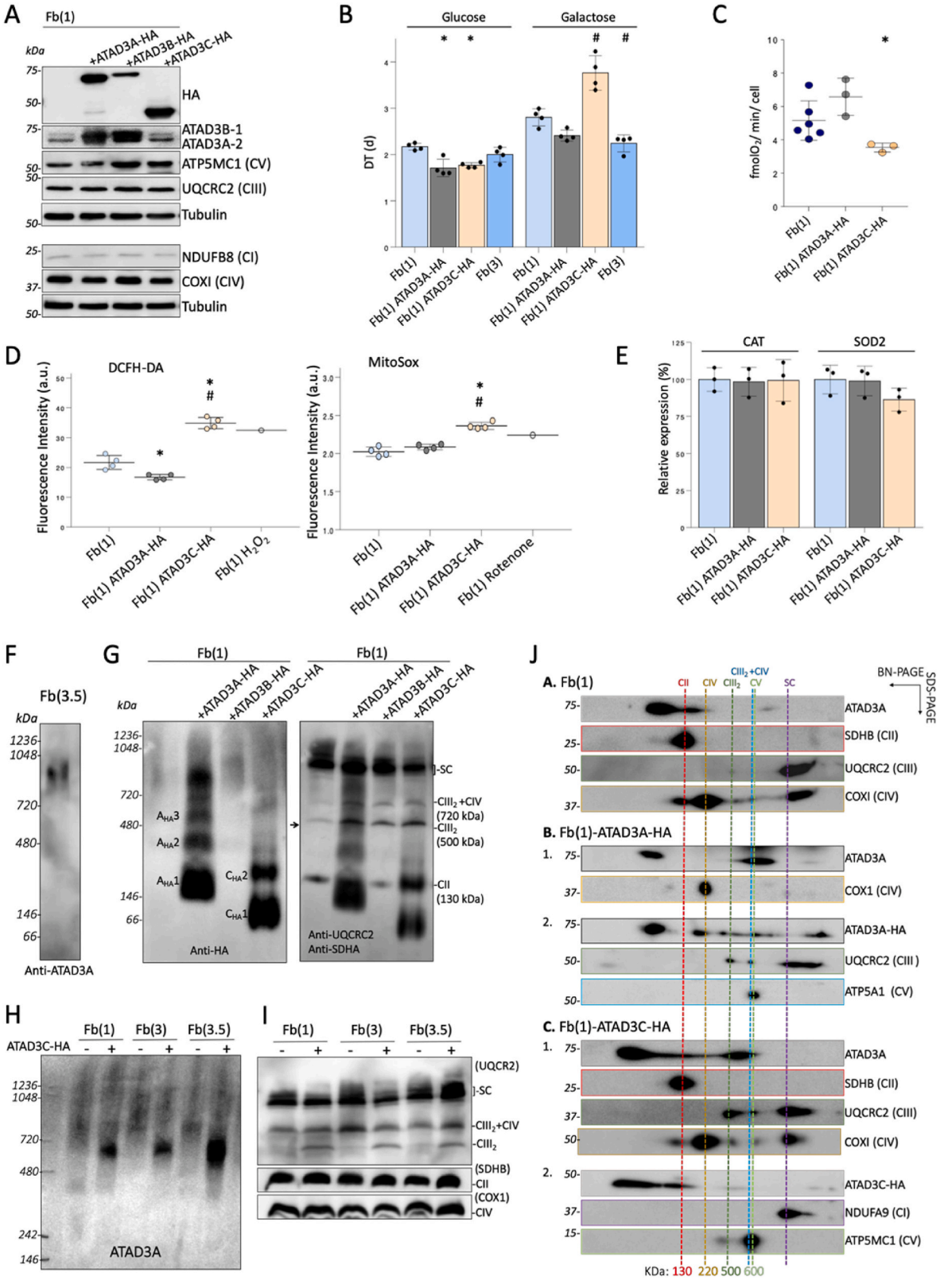

(caption on next page)

Fig. 3. ATAD3C is incorporated into ATAD3A membrane assemblies decreasing cellular oxidative phosphorylation.
A. Steady-state levels of HA tagged and respiratory chain proteins in fibroblasts Fb(1) and Fb(1) overexpressing ATAD3A-HA, ATAD3B-HA or ATAD3C-HA. Total cell lysates were resolved by SDS–PAGE and immunodetected with antibodies specific to -HA epitope, ATAD3A, ATAD3B and respiratory complex proteins as indicated. α-tubulin was used as loading control.
B. Doubling time (days) of fibroblasts Fb(1), Fb(3), and Fb(1) overexpressing ATAD3A-HA or ATAD3C-HA in glucose and galactose containing media. Data are presented as mean ± SD (n = 4). Statistical significance was evaluated with the non-parametric Mann-Whitney *U* test,*p < 0.05 (vs. Fb(1) glucose; #p < 0.05 (vs. Fb (1) galactose).
C. Basal oxygen consumption rate of fibroblasts Fb(1), and Fb(1) expressing ATAD3A-HA or ATAD3C-HA. Data are presented as mean ± SD. Statistical significance was evaluated with the non-parametric Mann-Whitney *U* test, *p < 0.05 (vs. Fb(1)).
D. Cell fluorescence intensity of DCFH-DA and MitoSOX probes measured by flow cytometry. Fluorescence data in arbitrary units (a.u.) are presented as mean ± SD. Data are presented as mean ± SD. Statistical significance was evaluated with the non-parametric Mann-Whitney *U* test, *p < 0.05 (vs. Fb(1)), #p < 0.05 (vs. Fb(1)-ATAD3A-HA).
E. Relative expression of CAT and SOD2 mRNAs in fibroblasts Fb(1) and Fb(1) expressing the HA-tagged version of ATAD3A and ATAD3C. Data are presented as mean ± SD. Statistical significance was evaluated with the non-parametric Mann-Whitney *U* test *p < 0.05 (vs. Fb(1) considered 100 %).
F. Detection of ATAD3A assembly in the mitochondrial membrane of human fibroblasts. Mitochondria were solubilized with digitonin and native complexes were resolved by BNGE and immunodetected with anti-ATAD3A.
G. Detection of ATAD3 assemblies in fibroblasts Fb(1) and Fb(1) expressing the HA-tagged version of ATAD3-palalogs. Mitochondria were solubilized with digitonin and native complexes were resolved by BNGE and immunodetected with specific anti-HA antibody followed by anti- UQCRC2 (CIII) and SDHB (CII) antibodies. The Mw of the main bands detected with anti-HA was estimated comparing their in-gel motility with that of respiratory complexes, $A_{HA}1$: 1,1 to 1,9 times the monomer size; $A_{HA}2$: 3.9 times the monomer size; $A_{HA}3$: 6.9 times the monomer size; $C_{HA}1$: 1 to 1.4 times the monomer size; $C_{HA}2$ band that could correspond to trimers.
H. Detection of the main ATAD3A assembly in the mitochondrial membrane of three human fibroblasts, Fb(1), Fb(3), and Fb(3.5), overexpressing or not ATAD3C-HA. Digitonin treated mitochondria were resolved by BNGE and immunodetected with anti-ATAD3A antibody.
I. Detection of native respiratory complexes in three human fibroblasts, Fb(1), Fb(3), and Fb(3.5) overexpressing or not ATAD3C-HA. Digitonin treated mitochondria were resolved by BNGE and immunodetected with specific antibodies: anti-UQCRC2, anti-COX1 and anti-SDHB sequentially.
J. Characterization of ATAD3 assemblies and OXPHOS complexes by two-dimensional electrophoresis in Fb(1), and Fb(1) expressing ATAD3A-HA or ATAD3C-HA. Mitochondrial fractions were extracted and separated by 1D-BNGE followed by 2D-PAGE. 1 and 2 indicate independent blots. Antibody hybridization was sequential for each blot. The positions of subunits of respiratory complexes CI, CII, and CIV, were used to align the immunoblots and correlate with the Mw in 1D-BNGE: CI holoenzyme (970 kDa), ATP synthase holoenzyme (600 kDa), ATP synthase dimer (1200 kDa), F1-ATPase subcomplex (370 kDa), complex III dimer (500 kDa), and complex IV monomer (200 kDa), respectively.

was also significantly higher, similar to that observed in as in fibroblasts in which $O_2^{\bullet}-$production was promoted by inhibition of complex I with rotenone [57] (Fig. 3D). However, since we did not perform specific identification of the 2-hydroxyethidium product [58] and, in an alternative approach, the *in vivo* expression of antioxidant enzyme systems such as mitochondrial SOD2 for $O_2^{\bullet\ -}$, and matrix catalase for H_2O_2, were not found to be increased (Fig. 3E), we could not conclude that cellular ROS generation occurred in mitochondria.

Collectively, these results indicate that overexpression of ATAD3A is well tolerated by the cells, whereas ATAD3C gain of function results in increased cellular ROS levels and reduced mitochondrial respiration, albeit with normal steady-state levels of multiple OXPHOS subunits.

3.6. ATAD3C is incorporated into membrane assemblies of ATAD3A and modifies the assembly pattern of respiratory complexes

To dissect the ATAD3 membrane assemblies, mitochondrial membranes were solubilized with digitonin and subjected to blue native electrophoresis (BNGE). In human fibroblast, endogenous ATAD3A was immunodetected in a large 800–900 kDa complex (Fig. 3F), as previously described [2,7].

When membranes of fibroblasts expressing ATAD3A-HA were analyzed, a pattern of at least four protein complexes with a broad mass distribution, containing the HA epitope, was immunodetected. To estimate the mass of these assemblies we compared their *in-gel* motility with that of digitonin-solubilized respiratory complexes [59] (Fig. 3G and Supplementary Fig. S10). ATAD3A-HA over-accumulated in a broad band with electrophoretic mobility compatible with monomers and dimers ($A_{HA}1$: 1,1 to 1,9 times the monomer size), followed by sub-assemblies compatible with tetramers ($A_{HA}2$: 3.9 times the monomer size) and heptamers ($A_{HA}3$: 6.9 times the monomer size) (Fig. 3G, Supplementary Fig. S10). These results could be compatible with oligomerization by union of dimers with tetramers to yield hexamers similar to those described for other AAA ATPases using techniques of analysis of purified proteins. Other peptides and/or membrane lipids should associate with them to form the large molecular weight ATAD3A complex.

When starting from fibroblasts expressing ATAD3C-HA, the HA signal accumulated significantly in two assemblies, one compatible with monomers ($C_{HA}1$: 1 to 1.4 times the monomer size), and a second one with a size that could correspond to trimers ($C_{HA}2$) (Fig. 3G). In contrast to ATAD3A-HA, high molecular weight ATAD3C-HA homoassemblies were not clearly identifiable, indicating a low tendency to form independent high molecular weight homoassemblies. This is consistent with the low dimerization tendency observed for ATAD3C in whole-cell homogenates. Remarkably, immunodetection of endogenous ATAD3A protein in cells expressing ATAD3C-HA revealed a reduction in the size of the major membrane assembly of ATAD3A, usually detected at 800–900 kDa. The mobility shift was observed in three independent fibroblast cell lines (Fig. 3H and Supplementary Fig. S11), suggesting that ATAD3C subunits may be replacing subunits of ATAD3A in the main oligomeric assembly. Subsequent immunodetection with specific antibodies against proteins of respiratory complexes showed no variation in the abundance of complexes II, or IV, but revealed accumulation of dimeric CIII ($CIII_2$) in ATAD3C gain of function cells, to the detriment of that assembled in respiratory supercomplexes (Fig. 3I).

To further examine ATAD3 assemblies, mitochondrial membranes solubilized with digitonin were resolved using two-dimensional (2D) BNGE. Immunoblots allowed better resolution of endogenous complexes and revealed that most of endogenous ATAD3A was found as part of two low molecular weight assemblies (Fig. 3J(A)). The large assembly of ATAD3A at 800–900 kDa was also detected. Subsequent immunodetection with specific antibodies against respiratory complexes showed that, consistent with what was observed in 1D-BNGE, in human fibroblasts complex III was found mainly in supercomplexes (Fig. 3J(A)).

When fibroblasts overexpressing ATAD3A-HA were analyzed by 2D-BNGE, a pattern of subcomplexes containing the HA epitope, similar to those observed by 1D-BNGE, was detected up to the 800–900 kDa complex. Overexpression of ATAD3A-HA resulted in increased steady-state levels of the 800–900 kDa assembly compared to control fibroblasts (Fig. 3J(B)). These observations confirmed that the overexpressed tagged isoform is integrated into the endogenous complex.

In fibroblasts overexpressing ATAD3C-HA, the 2D blots confirmed the reduction in the size of the 800–900 kDa ATAD3A assembly already observed in 1D-BNGE. Anti-HA immunoreactivity was detected at the

equivalent position, indicating the incorporation of ATAD3C-HA subunits to the assembly. ATAD3C-HA was also found in two low molecular weight subassemblies previously observed (Fig. 3J(C)). In these cells, CIII was accumulated as $CIII_2$ whereas in control fibroblasts or in those overexpressing ATAD3A-HA was mainly found in SC. The distribution of CII and CIV was not altered (Fig. 3J(C)).

These results demonstrate that ATAD3C disrupts the main ATAD3A complex in the mitochondrial membrane leading to impaired supramolecular organization of respiratory complexes.

4. Discussion

In this work, we used molecular and functional approaches to define the cellular activity of ATAD3C, a truncated paralog of ATAD3A. We estimate that the segmental duplications of *ATAD3A* to generate *ATAD3B* and *ATAD3BC* could have taken place during primate speciation, in the last 25–40 million years in the period when many segmental duplications arose in the human genome [60]. Our data suggest that *ATAD3C* gene generates a protein that negatively regulates the function of the protein it derives from. Interestingly, paralogs encoding a truncated form of the ancestral gene were recently identified as contributors to human brain evolution. In examples such as *SRGAP2C* and *ARHGAP11B,* segmental duplications were incomplete and truncations were generated that facilitated antagonistic interactions with the parental gene in the first case [38] or gave rise to new functions in the second case [36]. The segmental duplications in human *ATAD3* locus are involved in recurrent rearrangements associated with mitochondrial disease [28] whose severity highlights the importance of molecular and functional study of the ATAD3 paralogs. Whereas dominant or recessive *ATAD3A* variants have been reported in patients with mitochondrial disease, pathological variants affecting exclusively *ATAD3B* or *ATAD3C* genes have not been described. A subject with a deletion of *ATAD3C* and *ATAD3B*, not involving *ATAD3A*, was assigned a clinical diagnosis associated with a second heterozygous deletion suggesting that homozygous deletion of *ATAD3C* and *ATAD3B* does not have a substantial impact on phenotype [23].

ATAD3C has lower expression than ATAD3A or ATAD3B in post mitotic tissues, however, at the protein level we found ATAD3C peptides in the HEK 293T cell line, as described in a previous work [61], confirming that *ATAD3C* is a true paralog. Quantitative proteomic assays have also identified ATAD3C in human tissues (lung and tonsil) [62]. In HEK 293T cells, we also detected unique peptides compatible with ATAD3A or ATAD3B isoforms previously detected by immunodetection [3,27,34,63,64]. ATAD3C protein, with lower sequence homology to its paralogs, and lower expression, has not been detected with ATAD3 antibodies in immunoblots.

By biochemical fractionation and membrane extraction we defined ATAD3C as a mitochondrial membrane embedded protein. Since the sub-mitochondrial localization is important to elucidate the protein substrates of the enzyme, we used protease digestion assays to further define the membrane topology of the protein. ATAD3C N-terminus was sensitive to trypsin attack in isolated mitochondria suggesting that it is located outside of the mitochondria, whereas the C-terminus remained more resistant to trypsin and behaved as an IMS protein. Previous studies using proteolytic digestion of purified mitochondria also located the ATAD3A paralog N-terminus in the cytosol, however, they proposed that ATAD3A C-terminus is facing the matrix and that the protein spans both mitochondrial membranes [6,34,65]. In our assays, the endogenous ATAD3A protein behaved like an OMM and not like an IMM protein. The transmembrane domain required for mitochondrial targeting of ATAD3A or ATAD3B was determined using mutagenesis approaches [6,65]. As the domain is 100 % conserved in ATAD3C, the three paralogs would be expected to share the same membrane localization in the mitochondria. Co-IP results, indicating interaction between the paralogs, also suggest that they should be found in the same subcellular location. Moreover, ATAD3A has been linked to mammalian mitochondria-ER contact sites, known as mitochondria-associated membranes (MAM), where patches of ER membrane co-purify with mitochondria [18,26]. Remarkably, a proximity biotinylation proteomic approach that avoids biochemical fractionation specifically localized ATAD3A in the ER membrane and OMM proteomes, indicating that it is an OMM protein candidate to be resident of mitochondria-ER contact sites [66].

Among human genes, we detected that those with the highest identity to *ATAD3A*, *ATAD3B*, and *ATAD3C* based on their sequence are members of the AAA ATPase subfamily, considered cellular machines that function in diverse biological pathways by segregating protein substrates from stable environments such as organelles or multi-subunit complexes. Recent structures of substrate-bound complexes of several of these enzymes have revealed that the protomers form a hexameric closed spiral staircase encircling an unfolded substrate [12,15,67–69]. These structures support a model in which ATP hydrolysis at the tail end of the staircase is coupled with ATP binding at the leading end, and indicate a unified hand-over-hand translocation mechanism that appears conserved among AAA + ATPases [70]. In the active assembly, the nucleotide binding pocket lies in the interface between two protomers. The arginine finger of one protomer comes into close proximity to the nucleotide bound in the neighboring protomer. In this state, AAA + ATPases show elevated ATPase activity, which can be abolished by mutations of the arginine finger [11]. Remarkably, ATAD3C lacks the characteristic arginine finger (arginine position 1) present in ATAD3A and ATAD3B and highly conserved in most AAA + proteins [50]. This suggests that ATAD3C may lack the ATPase activity, although, based solely on homology other contributions to this function cannot be excluded [11].

Our data strongly suggest that ATAD3C paralog acts as specific ATAD3A oligomer modifier. In co-IP assays, ATAD3C interacted with ATAD3A and vice-versa suggesting the formation of hetero-oligomers containing subunits of both paralogs. SDS-PAGE separation of the IP samples, in non-reducing conditions, showed overexpressed ATAD3A-HA mainly in bands compatible with monomers and dimers, whereas overexpressed ATAD3C-HA was detected mainly as monomers with a smear at higher molecular weight. This indicates low tendency to homo-oligomerize for ATAD3C, since in these experiments the most likely partner is the overexpressed monomer. Finally, BNGE analysis of mitochondrial membranes confirmed the presence of ATAD3C subunits in ATAD3A membrane assemblies, since upon overexpression of ATAD3C, ATAD3A accumulated in a smaller assembly in which subunits or ATAD3C were detected. Using various analytical techniques for the study of purified proteins it has been established that monomers of AAA proteins form stable dimers and a dynamic model for the assembly-disassembly of oligomers has been proposed, in which generally, the association of dimers with tetramers generates hexamers at high levels of ATP and magnesium [71–75]. Dimers, tetramers, and hexamers of ATAD3A were previously observed in cells by cross-linking experiments [34]. Our native separation of mitochondrial membranes showed a broad distribution of overexpressed ATAD3A-HA in discrete bands, in the mass range of 120–900 kDa. According to their motility, the main bands could correspond to monomers-dimers and tetramers what could indicate the association of dimers with tetramers in the structural organization of ATAD3A. ATAD3A with the HA epitope was also found in the ATAD3A high molecular weight assembly, the main form of endogenous ATAD3A when extracted from mitochondrial membranes with digitonin. However, ATAD3C-HA was not found in homo-oligomers of high molecular weight, but rather in hetero-oligomers with ATAD3A.

Functionally, ATAD3C expression reduced fibroblast proliferation under oxidative conditions and basal oxygen consumption whereas ATAD3A over-expression had no noticeable impact. We conclude that a dominant negative function of ATAD3C through the hetero-oligomer formation with endogenous ATAD3A, similar to that observed when ATAD3A mutants are expressed in fibroblasts or in fly models [23], would explain these results. The N-terminal truncation together with the

lack of arginine finger in the AAA ATPase domain of ATAD3C would alter the function of the ATAD3A oligomers in the membrane.

At the molecular level, we found that *ATAD3C* gain of function led to the accumulation of dimeric complex III in the mitochondrial membrane, which appears to be caused by the reduction of $CIII_2$ assembled of into respiratory SC. Complex III is the mid-segment of the respiratory chain [76] and it is central for respiratory chain maturation and SC formation [77,78]. The main function of SC may be to avoid the loss of reducing power by maintaining the close proximity and favorable orientation of the key respiratory chain components, so that lower SC formation correlated with more mitochondrial ROS generation [79]. In our cellular models, lower SC formation also correlated with higher cellular ROS production. Study of patients with ATAD3A-deficient mitochondrial disease found that OXPHOS function was not severely impaired and that ATAD3A is not crucial for the assembly of respiratory complexes, although borderline deficiencies of OXPHOS enzymes have been observed in tissues or cell lines of some patients, [23,25,29]. Remarkably, SC together with ATP synthase were the first structures in which alterations were detected in muscle from *ATAD3* KO mice, following altered cristae shape [2]. Because we did not detect OXPHOS defects in fibroblasts overexpressing ATAD3A, we excluded that ATAD3C toxicity is due to excessive accumulation of an overexpressed protein in the mitochondrial membrane compromising membrane integrity. The most plausible scenario is that ATAD3C, through modification of the primary function of ATAD3A oligomers, disrupts proper membrane formation leading to an imbalance that reduces SC assembly.

In summary, using an approach with HA-tagged proteins we show that *ATAD3C* open reading frame contains relevant coding information and its relative level of expression with respect to ATAD3A may modulate its activity. Because ATAD3C can form hetero-oligomers with ATAD3A, we propose that the main role of ATAD3C is to negatively regulate ATAD3A function. ATAD3C did not show oligomerization properties similar to those of ATAD3A, indicating that the only role in the cell is through its interaction with ATAD3A. Further molecular studies are needed to determine which proteins are translocated through the ATAD3 oligomer and what is the molecular mechanism linking the ATAD3 locus to mitochondrial disease.

In conclusion, our study reveals that the hominid-specific *ATAD3C* gene has a potentially significant impact for ATAD3A function regulation and ATAD3C expression in developmental stages or other physiological situations should be considered in human mitochondrial disease.

Funding statement

This work was supported by grants funded by Instituto de Salud Carlos III (ISCIII-FIS-PI21/00229) and European Regional Development Fund (FEDER); Gobierno de Aragón (LMP22_21, Grupos Consolidados B33_20R) and FEDER 2014–2020 'Construyendo Europa desde Aragón; Precipita-FECYT Crowdfunding (PR194); Fundación Mutua Madrileña; and Asociación de Enfermos de Patología Mitocondrial (AEPMI). The CIBERER is an initiative of the ISCIII. The authors declare that no funds, grants, or other support were received during the preparation of this manuscript.

Contribution statement

All authors contributed to the study conception and design. PB-B, JM and ER-P conceived and a designed the study and interpreted the data. Material preparation and data collection and analysis were performed by PG, ET-M, NG-P and AS. The first draft of the manuscript was written by PB-B and all authors commented on previous versions of the manuscript. All authors read and approved the final manuscript.

Data availability

The datasets not included in supplementary material are available from the corresponding author on reasonable request.

Ethics approval

This study was performed in line with the principles of the Declaration of Helsinki. Approval was granted by the Ethics Committee of the Government of Aragón (CEICA) (PI21/323). The authors affirm that the fibroblast donors provided informed consent for participate in this research.

Web pages of the databases used

RefSeq: https://www.ncbi.nlm.nih.gov/refseq/; accessed April 4, 2021.

Expression Atlas: https://www.ebi.ac.uk/gxa/home; accessed April 17, 2023.

Human Protein Atlas: https://www.proteinatlas.org; accessed April 4, 2021.

Compliance with ethical standards

This study was approved by the ethics committee of the Government of Aragón (CEICA) and was performed in accordance with the ethical standards laid down in the Declaration of Helsinki.

Declaration of competing interest

The authors declare no competing interests.

Acknowledgements

Authors would like to acknowledge the use of Servicio General de Apoyo a la Investigación-SAI, Universidad de Zaragoza; the Proteomics Unit of Complutense University of Madrid that belongs to ProteoRed, PRB3-ISCIII, supported by grant PT17/0019 of the PE I + D + i 2013–2016, funded by ISCIII and ERDF, for the assistance with proteomic analysis; and Dr. Javier Godino, Servicio de Separación Celular y Citometría, Instituto de Aragonés de Ciencias de la Salud, Zaragoza, for his assistance with flow cytometry.

Appendix A. Supplementary data

Supplementary data to this article can be found online at https://doi.org/10.1016/j.freeradbiomed.2023.12.006.

References

[1] T. Arguello, S. Peralta, H. Antonicka, G. Gaidosh, F. Diaz, Y.T. Tu, et al., ATAD3A has a scaffolding role regulating mitochondria inner membrane structure and protein assembly, Cell Rep. 37 (12) (2021), 110139, https://doi.org/10.1016/j.celrep.2021.110139.

[2] S. Peralta, S. Goffart, S.L. Williams, F. Diaz, S. Garcia, N. Nissanka, et al., ATAD3 controls mitochondrial cristae structure in mouse muscle, influencing mtDNA replication and cholesterol levels, J. Cell Sci. 131 (13) (2018), https://doi.org/10.1242/jcs.217075.

[3] S. Li, D. Rousseau, ATAD3, a vital membrane bound mitochondrial ATPase involved in tumor progression, J. Bioenerg. Biomembr. 44 (1) (2012) 189–197, https://doi.org/10.1007/s10863-012-9424-5.

[4] A. Reyes, J. He, C.C. Mao, L.J. Bailey, M. Di Re, H. Sembongi, et al., Actin and myosin contribute to mammalian mitochondrial DNA maintenance, Nucleic Acids Res. 39 (12) (2011) 5098–5108, https://doi.org/10.1093/nar/gkr052.

[5] M. Hoffmann, N. Bellance, R. Rossignol, W.J. Koopman, P.H. Willems, E. Mayatepek, et al., C. elegans ATAD-3 is essential for mitochondrial activity and development, PLoS One 4 (10) (2009), e7644, https://doi.org/10.1371/journal.pone.0007644.

[6] B. Gilquin, E. Taillebourg, N. Cherradi, A. Hubstenberger, O. Gay, N. Merle, et al., The AAA+ ATPase ATAD3A controls mitochondrial dynamics at the interface of the inner and outer membranes, Mol. Cell Biol. 30 (8) (2010) 1984–1996, https://doi.org/10.1128/MCB.00007-10.

[7] T. Goller, U.K. Seibold, E. Kremmer, W. Voos, W. Kolanus, Atad3 function is essential for early post-implantation development in the mouse, PLoS One 8 (1) (2013), e54799, https://doi.org/10.1371/journal.pone.0054799.

[8] A.E. Frazier, A.G. Compton, Y. Kishita, D.H. Hock, A.E. Welch, S.S.C. Amarasekera, et al., Fatal perinatal mitochondrial cardiac failure caused by recurrent de novo duplications in the ATAD3 locus, Med (N Y). 2 (1) (2021) 49–73, https://doi.org/10.1016/j.medj.2020.06.004.
[9] T. Frickey, A.N. Lupas, Phylogenetic analysis of AAA proteins, J. Struct. Biol. 146 (1–2) (2004) 2–10, https://doi.org/10.1016/j.jsb.2003.11.020.
[10] P.I. Hanson, S.W. Whiteheart, AAA+ proteins: have engine, will work, Nat. Rev. Mol. Cell Biol. 6 (7) (2005) 519–529, https://doi.org/10.1038/nrm1684.
[11] P. Wendler, S. Ciniawsky, M. Kock, S. Kube, Structure and function of the AAA+ nucleotide binding pocket, Biochim. Biophys. Acta 1823 (1) (2012) 2–14, https://doi.org/10.1016/j.bbamcr.2011.06.014.
[12] A.H. de la Peña, E.A. Goodall, S.N. Gates, G.C. Lander, A. Martin, Substrate-engaged 26S proteasome structures reveal mechanisms for ATP-hydrolysis-driven translocation, Science 362 (6418) (2018), https://doi.org/10.1126/science.aav0725.
[13] H. Han, J.M. Fulcher, V.P. Dandey, J.H. Iwasa, W.I. Sundquist, M.S. Kay, et al., Structure of Vps4 with circular peptides and implications for translocation of two polypeptide chains by AAA+ ATPases, Elife 8 (2019), https://doi.org/10.7554/eLife.44071.
[14] L. Kater, N. Wagener, O. Berninghausen, T. Becker, W. Neupert, R. Beckmann, Structure of the Bcs1 AAA-ATPase suggests an airlock-like translocation mechanism for folded proteins, Nat. Struct. Mol. Biol. 27 (2) (2020) 142–149, https://doi.org/10.1038/s41594-019-0364-1.
[15] C. Puchades, A.J. Rampello, M. Shin, C.J. Giuliano, R.L. Wiseman, S.E. Glynn, et al., Structure of the mitochondrial inner membrane AAA+ protease YME1 gives insight into substrate processing, Science 358 (2017) 6363, https://doi.org/10.1126/science.aao0464.
[16] E.C. Twomey, Z. Ji, T.E. Wales, N.O. Bodnar, S.B. Ficarro, J.A. Marto, et al., Substrate processing by the Cdc48 ATPase complex is initiated by ubiquitin unfolding, Science 365 (6452) (2019), https://doi.org/10.1126/science.aax1033.
[17] D.F. Bogenhagen, D. Rousseau, S. Burke, The layered structure of human mitochondrial DNA nucleoids, J. Biol. Chem. 283 (6) (2008) 3665–3675, https://doi.org/10.1074/jbc.M708444200.
[18] J.M. Gerhold, Ş. Cansiz-Arda, M. Lõhmus, O. Engberg, A. Reyes, H. van Rennes, et al., Human mitochondrial DNA-protein complexes attach to a cholesterol-rich membrane structure, Sci. Rep. 5 (1) (2015), https://doi.org/10.1038/srep15292.
[19] J. He, C.C. Mao, A. Reyes, H. Sembongi, M. Di Re, C. Granycome, et al., The AAA+ protein ATAD3 has displacement loop binding properties and is involved in mitochondrial nucleoid organization, J. Cell Biol. 176 (2) (2007) 141–146, https://doi.org/10.1083/jcb.200609158.
[20] J. He, H.M. Cooper, A. Reyes, M. Di Re, H. Sembongi, T.R. Litwin, et al., Mitochondrial nucleoid interacting proteins support mitochondrial protein synthesis, Nucleic Acids Res. 40 (13) (2012) 6109–6121, https://doi.org/10.1093/nar/gks266.
[21] T. Ishihara, R. Ban-Ishihara, A. Ota, N. Ishihara, Mitochondrial nucleoid trafficking regulated by the inner-membrane AAA-ATPase ATAD3A modulates respiratory complex formation, Proc. Natl. Acad. Sci. U. S. A. 119 (47) (2022), e2210730119, https://doi.org/10.1073/pnas.2210730119.
[22] H.M. Cooper, Y. Yang, E. Ylikallio, R. Khairullin, R. Woldegebriel, K.L. Lin, et al., ATPase-deficient mitochondrial inner membrane protein ATAD3A disturbs mitochondrial dynamics in dominant hereditary spastic paraplegia, Hum. Mol. Genet. 26 (8) (2017) 1432–1443, https://doi.org/10.1093/hmg/ddx042.
[23] T. Harel, W.H. Yoon, C. Garone, S. Gu, Z. Coban-Akdemir, M.K. Eldomery, et al., Recurrent de novo and biallelic variation of ATAD3A, encoding a mitochondrial membrane protein, results in distinct neurological syndromes, Am. J. Hum. Genet. 99 (4) (2016) 831–845, https://doi.org/10.1016/j.ajhg.2016.08.007.
[24] M.B. Rone, A.S. Midzak, L. Issop, G. Rammouz, S. Jagannathan, J. Fan, et al., Identification of a dynamic mitochondrial protein complex driving cholesterol import, trafficking, and metabolism to steroid hormones, Mol. Endocrinol. 26 (11) (2012) 1868–1882, https://doi.org/10.1210/me.2012-1159.
[25] R. Desai, A.E. Frazier, R. Durigon, H. Patel, A.W. Jones, I. Dalla Rosa, et al., ATAD3 gene cluster deletions cause cerebellar dysfunction associated with altered mitochondrial DNA and cholesterol metabolism, Brain 140 (6) (2017) 1595–1610, https://doi.org/10.1093/brain/awx094.
[26] L. Issop, J. Fan, S. Lee, M.B. Rone, K. Basu, J. Mui, et al., Mitochondria-associated membrane formation in hormone-stimulated leydig cell steroidogenesis: role of ATAD3, Endocrinology 156 (1) (2015) 334–345, https://doi.org/10.1210/en.2014-1503.
[27] N. Merle, O. Féraud, B. Gilquin, A. Hubstenberger, S. Kieffer-Jacquinot, N. Assard, et al., ATAD3B is a human embryonic stem cell specific mitochondrial protein, re-expressed in cancer cells, that functions as dominant negative for the ubiquitous ATAD3A, Mitochondrion 12 (4) (2012) 441–448, https://doi.org/10.1016/j.mito.2012.05.005.
[28] A.C. Gunning, K. Strucinska, M. Muñoz Oreja, A. Parrish, R. Caswell, K.L. Stals, et al., Recurrent de novo NAHR reciprocal duplications in the ATAD3 gene cluster cause a neurogenetic trait with perturbed cholesterol and mitochondrial metabolism, Am. J. Hum. Genet. 106 (2) (2020) 272–279, https://doi.org/10.1016/j.ajhg.2020.01.007.
[29] S. Peralta, A. González-Quintana, M. Ybarra, A. Delmiro, R. Pérez-Pérez, J. Docampo, et al., Novel ATAD3A recessive mutation associated to fatal cerebellar hypoplasia with multiorgan involvement and mitochondrial structural abnormalities, Mol. Genet. Metabol. 128 (4) (2019) 452–462, https://doi.org/10.1016/j.ymgme.2019.10.012.
[30] S. Azova, F. Rajabi, B.P. Modi, L. Mansfield, M.M. Jonas, A. Drobysheva, et al., Graves' disease in a five-month-old boy with an unusual treatment course, J. Pediatr. Endocrinol. Metab. 34 (3) (2021) 401–406, https://doi.org/10.1515/jpem-2020-0549.
[31] C.M.P.C.D. Peeters-Scholte, P.N. Adama van Scheltema, F.J.C.M. Klumper, S.M. P. Everwijn, M. Koopmans, M.J.V. Hoffer, et al., Genotype-phenotype correlation in ATAD3A deletions: not just of scientific relevance, Brain 140 (11) (2017) e66, https://doi.org/10.1093/brain/awx239.
[32] Z.Y. Yap, Y.H. Park, S.B. Wortmann, A.C. Gunning, S. Ezer, S. Lee, et al., Functional interpretation of ATAD3A variants in neuro-mitochondrial phenotypes, Genome Med. 13 (1) (2021) 55, https://doi.org/10.1186/s13073-021-00873-3.
[33] L. Shu, C. Hu, M. Xu, J. Yu, H. He, J. Lin, et al., ATAD3B is a mitophagy receptor mediating clearance of oxidative stress-induced damaged mitochondrial DNA, EMBO J. 40 (8) (2021), e106283, https://doi.org/10.15252/embj.2020106283.
[34] J. Baudier, ATAD3 proteins: brokers of a mitochondria-endoplasmic reticulum connection in mammalian cells, Biol. Rev. 93 (2) (2018) 827–844, https://doi.org/10.1111/brv.12373.
[35] J.A. Bailey, Z. Gu, R.A. Clark, K. Reinert, R.V. Samonte, S. Schwartz, et al., Recent segmental duplications in the human genome, Science 297 (5583) (2002) 1003–1007, https://doi.org/10.1126/science.1072047.
[36] M.Y. Dennis, E.E. Eichler, Human adaptation and evolution by segmental duplication, Curr. Opin. Genet. Dev. 41 (2016) 44–52, https://doi.org/10.1016/j.gde.2016.08.001.
[37] T. Marques-Bonet, J.M. Kidd, M. Ventura, T.A. Graves, Z. Cheng, L.W. Hillier, et al., A burst of segmental duplications in the genome of the African great ape ancestor, Nature 457 (7231) (2009) 877–881, https://doi.org/10.1038/nature07744.
[38] C. Charrier, K. Joshi, J. Coutinho-Budd, J.E. Kim, N. Lambert, J. de Marchena, et al., Inhibition of SRGAP2 function by its human-specific paralogs induces neoteny during spine maturation, Cell 149 (4) (2012) 923–935, https://doi.org/10.1016/j.cell.2012.03.034.
[39] I.T. Fiddes, G.A. Lodewijk, M. Mooring, C.M. Bosworth, A.D. Ewing, G.L. Mantalas, et al., Human-specific NOTCH2NL genes affect notch signaling and cortical neurogenesis, Cell 173 (6) (2018) 1356–1369.e22, https://doi.org/10.1016/j.cell.2018.03.051.
[40] I.K. Suzuki, D. Gacquer, R. Van Heurck, D. Kumar, M. Wojno, A. Bilheu, et al., Human-specific NOTCH2NL genes expand cortical neurogenesis through delta/notch regulation, Cell 173 (6) (2018) 1370–1384.e16, https://doi.org/10.1016/j.cell.2018.03.067.
[41] E. Perales-Clemente, M.P. Bayona-Bafaluy, A. Pérez-Martos, A. Barrientos, P. Fernández-Silva, J.A. Enriquez, Restoration of electron transport without proton pumping in mammalian mitochondria, Proc. Natl. Acad. Sci. U. S. A. 105 (48) (2008) 18735–18739, https://doi.org/10.1073/pnas.0810518105.
[42] E. Fernández-Vizarra, G. Ferrín, A. Pérez-Martos, P. Fernández-Silva, M. Zeviani, J. A. Enríquez, Isolation of mitochondria for biogenetical studies: an update, Mitochondrion 10 (3) (2010) 253–262, https://doi.org/10.1016/j.mito.2009.12.148.
[43] R. Moreno-Loshuertos, J. Marco-Brualla, P. Meade, R. Soler-Agesta, J.A. Enriquez, P. Fernández-Silva, How hot can mitochondria be? Incubation at temperatures above 43 °C induces the degradation of respiratory complexes and supercomplexes in intact cells and isolated mitochondria, Mitochondrion 69 (2023) 83–94, https://doi.org/10.1016/j.mito.2023.02.002.
[44] L.G. Nijtmans, N.S. Henderson, I.J. Holt, Blue Native electrophoresis to study mitochondrial and other protein complexes, Methods 26 (4) (2002) 327–334, https://doi.org/10.1016/S1046-2023(02)00038-5.
[45] N.A. O'Leary, M.W. Wright, J.R. Brister, S. Ciufo, D. Haddad, R. McVeigh, et al., Reference sequence (RefSeq) database at NCBI: current status, taxonomic expansion, and functional annotation, Nucleic Acids Res. 44 (D1) (2016) D733–D745, https://doi.org/10.1093/nar/gkv1189.
[46] C.B. Stewart, T.R. Disotell, Primate evolution - in and out of Africa, Curr. Biol. 8 (16) (1998) R582–R588, https://doi.org/10.1016/s0960-9822(07)00367-3.
[47] J.M. Miller, E.J. Enemark, Fundamental characteristics of AAA+ protein family structure and function, Archaea 2016 (2016) 1–12, https://doi.org/10.1155/2016/9294307.
[48] J. Jumper, R. Evans, A. Pritzel, T. Green, M. Figurnov, O. Ronneberger, et al., Highly accurate protein structure prediction with AlphaFold, Nature 596 (7873) (2021) 583–589, https://doi.org/10.1038/s41586-021-03819-2.
[49] R.C. NCBI, Database resources of the national center for biotechnology information, Nucleic Acids Res. 46 (D1) (2018) D8–D13, https://doi.org/10.1093/nar/gkx1095.
[50] T. Ogura, S.W. Whiteheart, A.J. Wilkinson, Conserved arginine residues implicated in ATP hydrolysis, nucleotide-sensing, and inter-subunit interactions in AAA and AAA+ ATPases, J. Struct. Biol. 146 (1–2) (2004) 106–112, https://doi.org/10.1016/j.jsb.2003.11.008.
[51] C. GTEx, Human genomics. The Genotype-Tissue Expression (GTEx) pilot analysis: multitissue gene regulation in humans, Science 348 (6235) (2015) 648–660, https://doi.org/10.1126/science.1262110.
[52] I. Papatheodorou, P. Moreno, J. Manning, A.M. Fuentes, N. George, S. Fexova, et al., Expression Atlas update: from tissues to single cells, Nucleic Acids Res. 48 (D1) (2020) D77–D83, https://doi.org/10.1093/nar/gkz947.
[53] S.J. Lindsay, Y. Xu, S.N. Lisgo, L.F. Harkin, A.J. Copp, D. Gerrelli, et al., HDBR expression: a unique Resource for global and individual gene expression studies during early human brain development, Front. Neuroanat. 10 (2016) 86, https://doi.org/10.3389/fnana.2016.00086.
[54] M. Uhlen, M.J. Karlsson, W. Zhong, A. Tebani, C. Pou, J. Mikes, et al., A genome-wide transcriptomic analysis of protein-coding genes in human blood cells, Science 366 (2019) 6472, https://doi.org/10.1126/science.aax9198.

[55] C. Combet, C. Blanchet, C. Geourjon, G. Deléage, NPS@: network protein sequence analysis, Trends Biochem. Sci. 25 (3) (2000) 147–150, https://doi.org/10.1016/s0968-0004(99)01540-6.
[56] M.P. Murphy, How mitochondria produce reactive oxygen species, Biochem. J. 417 (1) (2009) 1–13, https://doi.org/10.1042/BJ20081386.
[57] L. Plecitá-Hlavatá, H. Engstová, J. Ježek, B. Holendová, J. Tauber, L. Petrásková, et al., Potential of mitochondria-targeted antioxidants to prevent oxidative stress in pancreatic β-cells, Oxid. Med. Cell. Longev. 2019 (2019), 1826303, https://doi.org/10.1155/2019/1826303.
[58] M.P. Murphy, H. Bayir, V. Belousov, C.J. Chang, K.J.A. Davies, M.J. Davies, et al., Guidelines for measuring reactive oxygen species and oxidative damage in cells and in vivo, Nat. Metab. 4 (6) (2022) 651–662, https://doi.org/10.1038/s42255-022-00591-z.
[59] I. Wittig, T. Beckhaus, Z. Wumaier, M. Karas, H. Schägger, Mass estimation of native proteins by blue native electrophoresis: principles and practical hints, Mol. Cell. Proteomics 9 (10) (2010) 2149–2161, https://doi.org/10.1074/mcp.M900526-MCP200.
[60] P. Stankiewicz, J.R. Lupski, Structural variation in the human genome and its role in disease, Annu. Rev. Med. 61 (2010) 437–455, https://doi.org/10.1146/annurev-med-100708-204735.
[61] A. Garin-Muga, L. Odriozola, A. Martínez-Val, N. Del Toro, R. Martínez, M. Molina, et al., Detection of missing proteins using the PRIDE database as a source of mass spectrometry evidence, J. Proteome Res. 15 (11) (2016) 4101–4115, https://doi.org/10.1021/acs.jproteome.6b00437.
[62] D. Wang, B. Eraslan, T. Wieland, B. Hallström, T. Hopf, D.P. Zolg, et al., A deep proteome and transcriptome abundance atlas of 29 healthy human tissues, Mol. Syst. Biol. 15 (2) (2019), https://doi.org/10.15252/msb.20188503.
[63] A. Hubstenberger, G. Labourdette, J. Baudier, D. Rousseau, ATAD 3A and ATAD 3B are distal 1p-located genes differentially expressed in human glioma cell lines and present in vitro anti-oncogenic and chemoresistant properties, Exp. Cell Res. 314 (15) (2008) 2870–2883, https://doi.org/10.1016/j.yexcr.2008.06.017.
[64] S. Li, F. Lamarche, R. Charton, C. Delphin, O. Gires, A. Hubstenberger, et al., Expression analysis of ATAD3 isoforms in rodent and human cell lines and tissues, Gene 535 (1) (2014) 60–69, https://doi.org/10.1016/j.gene.2013.10.062.
[65] A. Hubstenberger, N. Merle, R. Charton, G. Brandolin, D. Rousseau, Topological analysis of ATAD3A insertion in purified human mitochondria, J. Bioenerg. Biomembr. 42 (2) (2010) 143–150, https://doi.org/10.1007/s10863-010-9269-8.
[66] V. Hung, S.S. Lam, N.D. Udeshi, T. Svinkina, G. Guzman, V.K. Mootha, et al., Proteomic mapping of cytosol-facing outer mitochondrial and ER membranes in living human cells by proximity biotinylation, Elife 6doi (2017), https://doi.org/10.7554/eLife.24463.
[67] I. Cooney, H. Han, M.G. Stewart, R.H. Carson, D.T. Hansen, J.H. Iwasa, et al., Structure of the Cdc48 segregase in the act of unfolding an authentic substrate, Science 365 (6452) (2019) 502–505, https://doi.org/10.1126/science.aax0486.
[68] H. Han, N. Monroe, W.I. Sundquist, P.S. Shen, C.P. Hill, The AAA ATPase Vps4 binds ESCRT-III substrates through a repeating array of dipeptide-binding pockets, Elife 6doi (2017), https://doi.org/10.7554/eLife.31324.
[69] Z.A. Ripstein, R. Huang, R. Augustyniak, L.E. Kay, J.L. Rubinstein, Structure of a AAA+ unfoldase in the process of unfolding substrate, Elife 6 (2017), https://doi.org/10.7554/eLife.25754.
[70] P.S. Shen, Rearranging AAA+ architecture to accommodate folded substrates, Nat. Struct. Mol. Biol. 27 (3) (2020) 225–226, https://doi.org/10.1038/s41594-020-0389-5.
[71] M. Babst, B. Wendland, E.J. Estepa, S.D. Emr, The Vps4p AAA ATPase regulates membrane association of a Vps protein complex required for normal endosome function, EMBO J. 17 (11) (1998) 2982–2993, https://doi.org/10.1093/emboj/17.11.2982.
[72] C. Bieniossek, T. Schalch, M. Bumann, M. Meister, R. Meier, U. Baumann, The molecular architecture of the metalloprotease FtsH, Proc. Natl. Acad. Sci. U. S. A. 103 (9) (2006) 3066–3071, https://doi.org/10.1073/pnas.0600031103.
[73] W. Kress, H. Mutschler, E. Weber-Ban, Assembly pathway of an AAA+ protein: tracking ClpA and ClpAP complex formation in real time, Biochemistry 46 (21) (2007) 6183–6193, https://doi.org/10.1021/bi602616t.
[74] T. Maisel, S. Joseph, T. Mielke, J. Bürger, S. Schwarzinger, O. Meyer, The CoxD protein, a novel AAA+ ATPase involved in metal cluster assembly: hydrolysis of nucleotide-triphosphates and oligomerization, PLoS One 7 (10) (2012), e47424, https://doi.org/10.1371/journal.pone.0047424.
[75] A.J. Serban, I.L. Breen, H.Q. Bui, M. Levitus, R.M. Wachter, Assembly-disassembly is coupled to the ATPase cycle of tobacco Rubisco activase, J. Biol. Chem. 293 (50) (2018) 19451–19465, https://doi.org/10.1074/jbc.RA118.005047.
[76] J.A. Letts, L.A. Sazanov, Clarifying the supercomplex: the higher-order organization of the mitochondrial electron transport chain, Nat. Struct. Mol. Biol. 24 (10) (2017) 800–808, https://doi.org/10.1038/nsmb.3460.
[77] E. Fernández-Vizarra, S. López-Calcerrada, L.E. Formosa, R. Pérez-Pérez, S. Ding, I. M. Fearnley, et al., SILAC-based complexome profiling dissects the structural organization of the human respiratory supercomplexes in SCAFI^{KO} cells, Biochim. Biophys. Acta Bioenerg. 1862 (7) (2021), 148414, https://doi.org/10.1016/j.bbabio.2021.148414.
[78] M. Protasoni, R. Pérez-Pérez, T. Lobo-Jarne, M.E. Harbour, S. Ding, A. Peñas, et al., Respiratory supercomplexes act as a platform for complex III-mediated maturation of human mitochondrial complexes I and IV, EMBO J. 39 (3) (2020), e102817, https://doi.org/10.15252/embj.2019102817.
[79] I. Lopez-Fabuel, J. Le Douce, A. Logan, A.M. James, G. Bonvento, M.P. Murphy, et al., Complex I assembly into supercomplexes determines differential mitochondrial ROS production in neurons and astrocytes, Proc. Natl. Acad. Sci. U. S. A. 113 (46) (2016) 13063–13068, https://doi.org/10.1073/pnas.1613701113.